ACS APPLIED MATERIALS & INTERFACES

RESEARCH ARTICLE

www.acsami.org

Poly(3,4-ethylenedioxythiophene)-Ionic Liquid Functionalized Graphene/Reduced Graphene Oxide Nanostructures: Improved Conduction and Electrochromism

Aditya P. Saxena,[†] Melepurath Deepa,[*,‡] Amish G. Joshi,[†] Shweta Bhandari,[†] and Avanish Kumar Srivastava[†]

[†]National Physical Laboratory, Dr. K.S. Krishnan Road, New Delhi, 110012 India

[‡]Department of Chemistry, Indian Institute of Technology Hyderabad, Ordnance Factory Estate, Yeddumailaram, 502205, Andhra Pradesh, India

Supporting Information

ABSTRACT: Nanocomposite assemblies of poly(3,4-ethylenedioxythiophene) (PEDOT), embedded with (a) fluoro alkyl phosphate based ionic liquid functionalized graphene (ILFG) and (b) reduced graphene oxide (RGO) prepared from a modified Hummers' method, have been synthesized. Defect free graphene nanosheets within the size of a few nanometers were achieved in the PEDOT−ILFG nanocomposite. In contrast, structures comprising graphene oxide wrinkles interspersed with the amorphous polymer were obtained in the PEDOT−RGO nanocomposite. X-ray photoelectron spectroscopy showed that neat ILFG was considerably less oxidized as compared to the neat RGO, which ratified the superiority of the ionic liquid functionalization strategy over the conventional chemical approach, for exfoliating graphite. Substantially higher electrochemical activity, improved ionic/electronic conductivity, much faster switching rates, and an almost ballistic enhancement in the electrochromic coloration efficiency attained for the PEDOT−ILFG nanocomposite in comparison to PEDOT−RGO film were irrefutable proofs that demonstrated the ability of the ionic liquid to not only fortify the structure of graphene but also facilitate charge transport through the bulk of the film, by providing less impeded pathways. Since PEDOT−ILFG/-RGO nanocomposites of good uniformity have been achieved, this, to some extent, addresses the challenge associated with the processing of graphene based high performance materials for practical applications.

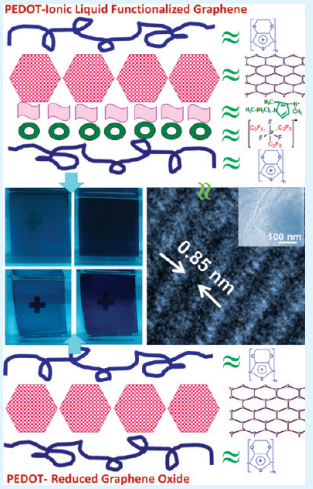

KEYWORDS: poly(3,4-ethylenedioxythiophene), electrochromic, graphene oxide, ionic liquid

1. INTRODUCTION

Conjugated electroactive polymers have sparked considerable interest as they find a gamut of applications in solid state devices such as supercapacitors,[1−3] sensors,[4−7] batteries,[8] organic or dye-sensitized solar cells,[9−11] corrosion control,[12] drug delivery,[13] photovoltaic,[14] electrochromic cells,[15] and actuators.[16,17] Among these diverse applications, conducting polymer based electrochromic cells are attractive, as they are cheap and offer small response times and high contrast ratios. Furthermore, they also permit reversible conversion between two or more colors and can be prepared easily by chemical or electrochemical routes.[18,19] The π-conjugated backbone of the polymer provides a perfect environment for the incorporation of a number of organic and inorganic moieties to yield functional hybrid materials. Poly(3,4-ethylenedioxythiophene), or PEDOT, in particular, has stimulated much interest as a cathodic electrochrome due to fast switching between deep-blue and pale-blue hues, large electronic conductivity, high transmissivity for visible radiation, and resistance to degradation in the doped form.[20,21]

In the past, conducting polymer composites encompassing carbon nanotubes (CNTs) or quantum dots have been synthesized, as a blend of enhanced mechanical, surface, thermal, and electrical properties can be achieved due to the synergistic effects of the polymer and the nanomoiety.[22−27] However, a major practical shortcoming in utilizing CNTs is their tendency to aggregate. Graphene sheets (which are stacked one atom thick planar layer of sp^2 bonded carbon atoms), on the other hand, have certain advantages over CNTs, as they possess a π-electronic surface, and as a consequence, there is no need of helicity control. Moreover, CNTs are expensive as compared to graphene sheets, and it is easier to synthesize the latter. Graphene sheets are also characterized by a number of remarkable properties such as high fracture strength (125 GPa), Young's modulus (~1100 GPa), mobility of charge carriers (200 000 $cm^2\ V^{-1}\ s^{-1}$), thermal conductivity (~5000 $W\ m^{-1}\ K^{-1}$), and specific surface area (>2500 $m^2\ g^{-1}$), which render them suitable for a variety of applications.[28] In a previous report, Wang et al.[29] synthesized flexible, self-supporting composite paper made of graphene and

Received: December 21, 2010
Accepted: February 28, 2011
Published: March 17, 2011

polyaniline with very high tensile strength and electrochemical capacitance that outperformed conventional carbon based electrodes. In another report, Wang et al.[30] studied the fluorescence quenching of polythiophenes by graphene and showed the suitability of this material for organic bulk heterojunction solar cells. Further, graphene−PEDOT−polystyrene sulfonate (PEDOT/PSS)/PEDOT based hybrid materials have also been made, for use as transparent conducting electrodes, as these show electrical conductivity of the order of 0.2 S cm^{-1} and good distensibility.[31−33] In a recent study, composites of graphene have been shown to increase power efficiency in heterojunction solar cells.[34]

To the best of our knowledge, reports on electrochemistry and electrochromism of PEDOT−graphene nanocomposite films are rare. Here, we report the syntheses of PEDOT−graphene nanosheet films, by use of two different strategies. In the first one, we exfoliated graphite rods by an electrochemical route;[35] in a waterproof ionic liquid, 1-hexyl-2,3-dimethylimidazolium tris-(pentafluoroethyl) trifluorophosphate and ionic liquid functionalized graphene (ILFG) was obtained. This is the first report on the functionalization of graphene by a fluoroalkyl phosphate (FAP) based ionic liquid. In the second route, we synthesized reduced graphene oxide (RGO), from a modified Hummers' method.[36] Nanocomposites of (a) RGO with PEDOT and (b) ILFG with PEDOT were prepared in the form of thin films. The objective of this study has been to compare the two films in terms of their structure and redox chemistry and, in particular, to demonstrate the potential of the PEDOT−ILFG nanocomposite film, for practical electrochromic applications.

2. EXPERIMENTAL SECTION

2.1. Chemicals. 3,4-Ethylenedioxythiophene or EDOT (Aldrich) and ionic liquid (IL) 1-hexyl-2,3-dimethylimidazolium tris(pentafluoroethyl) trifluorophosphate (Merck) were used as received. Inorganic transparent electrodes of SnO_2/F-coated glass (Pilkington, sheet resistance: 14 Ω/sq) were cleaned in a soap solution, 30% HCl solution, double distilled water, and acetone (in that order) prior to use. Deionized water (resistivity ∼ 18.2 MΩ cm) obtained through a Milli-Q system and ethanol (Merck) were used as solvents. Sulfuric acid (H_2SO_4), nitric acid (HNO_3), hydrazine (N_2H_4), and ammonia (NH_3), all procured from Merck, were used as received.

2.2. Reduced Graphene Oxide (RGO). Two grams of graphite powder (<150 μm) was dispersed in a solution composed of H_2SO_4/HNO_3 mixed in a 3:1 volume ratio (12 mL of H_2SO_4 and 4 mL of HNO_3) and refluxed at 40 °C for 16 h. The resulting solution was ultrasonicated and centrifuged, and the dark brown precipitate was washed with deionized water until the pH was reduced to 5−6. The graphene oxide (GO) thus obtained was dried in air at 60 °C and then resuspended in deionized water to create a 0.07 wt % GO dispersion. To 40 mL of this GO dispersion, 0.024 mL of hydrazine solution (25% in water) and 0.18 mL of ammonia solution (25% in water) were added. The formulation was refluxed at 90−95 °C for 1 h in an oil bath. The solution was centrifuged, and the precipitate (reduced graphene oxide or RGO) was washed with deionized water and then dried at 60 °C in an oven and stored in air.

2.3. Ionic Liquid Functionalized Graphene (ILFG). Two graphite rods of 6 mm diameter and approximately 4 cm length were partially immersed in a solution of 10 g of 1-hexyl-2,3-dimethylimidazolium tris(pentafluoroethyl) trifluorophosphate and 0.8 wt % of deionized water (0.8 g) in a rectangular glass cuvette (5 cm × 1 cm × 5 cm). A dc potential of 16 V was applied to the graphite rods, and they were subjected to continuous corrosion at room temperature for 6 h. The resulting black-brown colloid was subjected to iterative centrifugation and washing with iso-propanol to remove the superfluous ionic liquid until neat ILFG was produced.

2.4. PEDOT−RGO and PEDOT−ILFG Films. A colloidal dispersion of 0.20 g of RGO solution (10 mg/mL) with 0.1 M EDOT in 20 mL of ethanol was used for preparation of the PEDOT−RGO films. A solution of 0.6 g of ILFG with 0.1 M EDOT in 20 mL of ethanol was used for PEDOT−ILFG films. Both solutions were ultrasonicated for 1 h prior to use. A three electrode system with a platinum rod as counter electrode and Ag/AgCl/KCl as a reference electrode and a transparent conducting SnO_2/F coated glass substrate as the working electrode was employed for film deposition. A constant potential of +1.5 V was applied to the working electrode which was immersed in an EDOT−RGO or EDOT−ILFG suspension for 300 s at room temperature. The resulting blue colored nanocomposite films of PEDOT−ILFG or PEDOT−RGO were immediately rinsed with ethanol and dried in air for 2 h and stored in air.

2.5. Characterization Techniques. The surface morphological features of the films were investigated using a scanning electron microscope (SEM, LEO 440). From cross-sectional SEM views (Figure S1, Supporting Information), the average thickness of the PEDOT−RGO film was deduced to be ∼650 nm and that of PEDOT−ILFG film was approximately 600 nm. For transmission electron microscopy (TEM), a thin layer of the sample was carefully extracted using forceps in deionized water and then transferred onto a carbon coated copper grid of 3.05 mm in diameter, and the solvent was evaporated at room temperature before use. TEM was carried out by employing a high resolution transmission electron microscopy (HRTEM) Tecnai G2F30 STWIN with a FEG source at 300 kV. Atomic force microscopy (AFM) images of the nanocomposite films were taken on a Veeco system, in noncontact mode, and these are shown in Figure S2, Supporting Information. X-ray photoelectron spectroscopy (XPS) was carried out on a Perkin-Elmer 1257 model operating at a base pressure of 4.2×10^{-8} Torr for as-synthesized PEDOT−RGO and PEDOT−ILFG films at 300 K with a nonmonochromatized Al Kα line at 1486.6 eV, an analyzer pass energy of 60 eV, and a hemispherical sector analyzer capable of 25 meV resolution. The overall instrumental resolution was about 0.3 eV. The core level spectra were deconvoluted using a nonlinear iterative least-squares Gaussian fitting procedure. For all fitting multiplets, the FWHMs were fixed accordingly. Corrections due to charging effects were taken care of by the use of C(1s) as an internal reference and the Fermi edge of a gold sample. For recording the valence band spectra, the step size was 0.026 eV, the time per step was 100 ms, and ten sweeps were performed for each sample. Cyclic voltammetry (CV) for the films was performed in a classical three electrode electrochemical cell within ±1 V, wherein a nanocomposite film was used as the working electrode, Ag/AgCl/KCl was employed as the reference electrode, and a Pt rod was used as the auxiliary electrode in the neat ionic liquid: 1-hexyl-2,3-dimethylimidazolium tris(pentafluoroethyl) trifluorophosphate, working as an electrolyte. The electronic conductivities of PEDOT−RGO films and PEDOT−ILFG films were obtained by transferring the films from the substrates into a circular cavity of fixed area (diameter = 0.4 cm) in the center of a sample holder made of mica of a definite thickness and sandwiching the same between two stainless steel electrodes, which in turn were insulated from one another by Teflon rings. $I-V$ characteristics were obtained by linear sweep voltammetry (LSV), wherein the voltage was swept from −3 to +3 V. The optical density for coloration efficiency calculations was measured in a Perkin-Elmer Lambda 25 spectrophotometer in the neat ionic liquid. Electrochemical impedance spectroscopy (EIS) was performed in the same three electrode configuration as the one employed for cyclic voltammetry, under different dc potentials superimposed over a sinusoidal ac amplitude of 10 mV in the neat ionic liquid: 1-hexyl-2,3-dimethylimidazolium tris(pentafluoroethyl) trifluorophosphate, in the frequency range of 1 MHz to 0.01 Hz. All electrochemical measurements and electropolymerization was performed

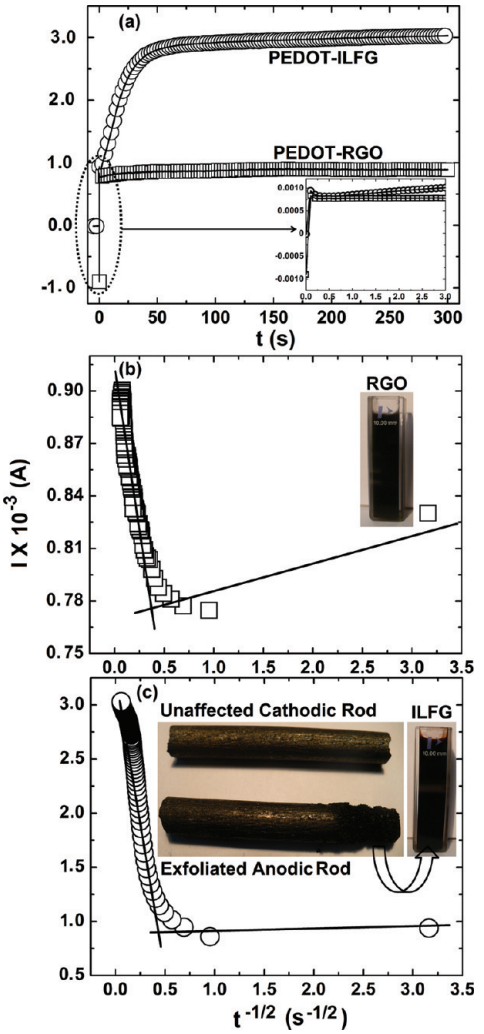

Figure 1. (a) Current−time transients for oxidative electropolymerization of 0.1 M 3,4-(ethylenedioxythiophene) manifesting in PEDOT−RGO (□) and PEDOT−ILFG (○) nanocomposite films. (b) and (c) are the corresponding Cottrell plots for PEDOT−RGO and PEDOT−ILFG films; the lines represent linear fits. Inset of (b) is a photograph of suspension of neat RGO in ethanol, and inset of (c) includes cathodic and anodic graphitic rods after exfoliation and suspension of neat ILFG in ethanol.

on a Gamry reference 600 potentiostat/galvanostat/ZRA with PHE 200/EIS 300 software.

3. RESULTS AND DISCUSSION

3.1. Exfoliation of Graphite and Chronoamperometry. The current−time transients for electropolymerization from suspensions containing the monomer and neat ILFG or neat RGO, under a constant potential of +1.5 V applied for ∼300 s, are shown in Figure 1. Prior to film preparation, in the electrosynthesis of neat ILFG, evidence for the exfoliation of graphite rod in the ionic liquid was obtained in the form of the corroded anodic graphite rod, which is in stark contrast to the cathodic graphite rod, that remains smooth and is unaffected by the prolonged application of dc potential (inset of Figure 1c). On the other hand, exfoliation of graphite (particle size <150 μm) by treatment with acids, followed by reduction with hydrazine, yielded reduced graphene oxide (neat RGO). Insets of Figure 1b,c show the colloidal suspensions of neat RGO in ethanol and neat ILFG in ethanol. These solutions were utilized for preparation of nanocomposite films with EDOT. Figure S3 (Supporting Information) shows the exfoliation process. Figure 1a shows that $t = 0$ s, the instant that potential is applied and current rises abruptly up to acquire a maximum of 7.8×10^{-4} A for the PEDOT−RGO nanocomposite; this current maximum is slightly greater for the PEDOT−ILFG nanocomposite: it is 9.5×10^{-4} A (inset of Figure 1a). The initial current spike is attributed to the double-layer capacitance charge. A plateaulike current response follows for both the nanocomposites. A similar trend was observed by Randriamahazaka et al.[37] for PEDOT doped by tetrabutyl ammonium perchlorate in acetonitrile. As shown in Figure 1a, the PEDOT−ILFG nanocomposite shows a gradual increase in the current initially prior to the acquisition of the plateaulike response unlike the PEDOT−RGO nanocomposite, wherein, no such trend was observed. At t = 55 s, the current acquires saturation and the value is 0.003 A for the PEDOT−ILFG film. In contrast, current saturates to a value of about 8×10^{-4} A after 10 s for the PEDOT−RGO film. It can be inferred that the first step, the process involving the formation of oligomers at the electrode−precursor sol interface, is less efficient in the PEDOT−RGO film as compared to the PEDOT−ILFG nanocomposite. The net electropolymerization charge deduced for the PEDOT−ILFG film is 875 mC cm^{-2}, and it is considerably higher than that for the PEDOT−RGO film (262 mC cm^{-2}) for the same duration of deposition, thus implying a higher electrodeposition efficiency in the former. From the chronoamperometry curves, the current (I) versus inverse of square root of time ($t^{-1/2}$) plots were derived and these are shown in Figure 1b,c. The apparent diffusion coefficient (D), has been calculated using Cottrell's equation

$$I = n \times F \times A \times c \times D^{1/2} \times \pi^{-1/2} \times t^{-1/2} \qquad (1)$$

where D is the apparent diffusion coefficient for the ionic species in units cm^2 s^{-1} and t is the time in s. For the PEDOT−RGO nanocomposite, D was rather low, with a value of 5.9×10^{-19} cm^2 s^{-1} in the early stages (corresponding to the migration of oligomeric species and graphene based anions), and for the region corresponding to the growth of the polymer, D increased by almost 6 orders of magnitude with a value of 8.7×10^{-12} cm^2 s^{-1}. D is relatively higher with magnitudes of 7.3×10^{-14} cm^2 s^{-1} and 9.7×10^{-11} cm^2 s^{-1} for the same zones during the growth of the PEDOT−ILFG nanocomposite. During the electropolymerization process, both the oligomeric species and charged graphene nanosheets (ionic liquid functionalized and equipped with $\{(C_2F_5)_3PF_3\}^-$ groups/in oxide form with COO^- groups) are adsorbed onto the substrate, and due to the heterogeneous nature of the initial layer and the increased surface area afforded by the graphene nanosheets, the oligomer to polymer transformation is rapid. The ionic liquid anion (in ILFG) is more effective as a counterion in contrast to the carboxylate ion (in RGO), which is obvious from the apparent diffusion coefficient. It renders a higher nucleation rate that accelerates the rate of polymer formation and also increases the thickness of the polymer deposit, for the same value of external bias.

3.2. SEM, HRTEM, and AFM Investigations. The SEM image of neat ionic liquid functionalized graphene (ILFG), in Figure 2a, shows the exfoliated graphene layers to be stacked one over the other, and at the peripheries (inset of Figure 2a), a ripplelike effect is seen; the layers appear discrete and can be visualized as

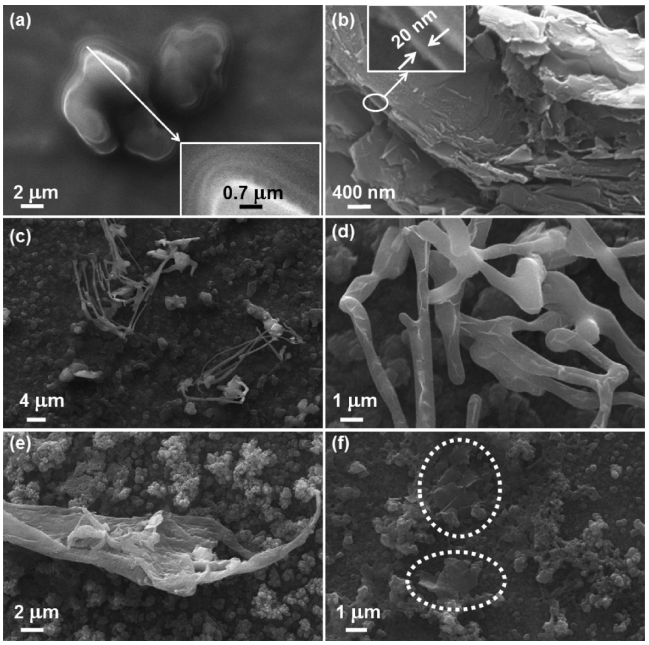

Figure 2. SEM images of (a) neat RGO and (b) neat ILFG; insets show magnified views of the peripheries. (c) Low and (d) high magnification images of PEDOT−ILFG nanocomposite; (e) and (f) are images of the PEDOT−RGO nanocomposite. The ellipses in (f) ensconce the RGO flakes in the composite.

monolayers. The average length of the graphene layer is about a few micrometers; however, the layer thickness has been determined from HRTEM images. Similar aggregation into thicker flakes has been observed previously by Gao et al.[38] The stacking of the layers is thicker in graphene oxide prepared by exfoliation of graphite in an acidic medium. For reduced graphene oxide (Figure 2a), the morphology is predominantly in the form of crumpled sheets. These platelet-like flat structures are thick, as functional groups such as epoxy, hydroxyl, ether, and carboxyl flank the nanosheets on each side, thus promoting their stacking. These functional groups also cause the digression from a perfectly conjugated structure to one composed of lattice defects, which manifests in folds and striations (Figure 2a). The ionic functionalized graphene has a relatively "distortion free" flattened structure (Figure 2b). The PEDOT−ILFG (Figure 2c) film is characterized by an interconnected network of grains and pores, typical of conducting polymers, synthesized by electropolymerization.[39] However, in addition, some elongated and intertwined artifacts embedded in the polymer matrix are also seen in this film. These novel shapes stem from the ionic liquid functionalized graphene. A magnified view of these unique shapes is presented in Figure 2d; these are several micrometers long, and their width lies between 200 and 700 nm; the branched streaks run along their entire lengths. The effect of these shapes is also reflected in the enhanced electrochromism and electrochemical activity of the films. Figure 2e shows that the PEDOT−RGO film has a dense compact morphology, and crumpled folded graphene oxide layers are superimposed on the polymer structure. Figure 2f, also from the same film, reveals the presence of graphene oxide flakes impregnated in the polymer matrix. These flakes are characterized by a width in the range of 0.5−1 μm.

The HRTEM image of neat ILFG in Figure 3a shows the presence of monolayers of ionic liquid functionalized graphene, which appear as crinkled silklike sheets and are a few hundred nanometers long. The darker portion of the image shows that the ILFG sheet in that region is more than one atom thick. From the right-hand side inset of the panel in Figure 3a, the thickness of the nanosheet, deduced at a point, where it is folded upward, is 1.1 nm. This is similar to a reported value of 1.1 nm,[35] for graphene oxide prepared in a hydrophilic ionic liquidlike 1-octyl-3-methylimidazoliumtetrafluoroborate, and for graphene oxide synthesized by a modified Hummers' method, the layer thickness is ∼1 nm.[38] In addition, some aggregated flakes were also seen, and these have been magnified in the left-hand side inset of Figure 3a. The flake size ranges between 10 and 15 nm. Figure 3b is a HRTEM image of RGO, and the graphene oxide layers are interspersed with folds; these folds are almost uniform in their width, as can be gauged from a localized view of the sample. Inset of Figure 3b shows this width to be of the order of 4 nm. The HRTEM image of the PEDOT−RGO film in Figure 3c, surprisingly, shows no striking feature; the observed granular-porous microstructure is typical of conducting polymers, albeit the presence of some slight crinkles (encircled in ellipses), and these probably arise from RGO. The PEDOT−ILFG film, on the other hand, at a low magnification, shows a structure composed of elongated shapes juxtaposed with regular grains (Figure 3d). The HRTEM image of this nanocomposite shows lattice fringes, in some portions. The enlarged view of the fringes is an indicator of an ordering of the structure, wherein the interplanar spacing is deduced to be 0.9 nm. This was further confirmed from a lattice scale image of a higher quality crystallite (i.e., it has fewer defects), shown in Figure 3f, wherein the moiré fringes of ILFG are well-resolved and the spacing is ∼0.85 nm. The overlapping of graphene nanosheets produces these fringes. It is well-known that the appearance of moiré fringes is due to the overlap of thin and tiny crystals in such a way, and therefore, certain planes of both the crystals produce interference fringes in real space. In the present micrograph, moiré fringes can be described as translational because they are parallel, thus signifying that graphene nanosheets are a part of the polymer film. Although a van der Waals' thickness of 0.34 nm has been reported for graphene,[35] here, the ionic liquid cations entrapped between two adjacent graphene nanosheets increase the separation. Additional SEM/TEM images are provided in Figure S4, Supporting Information.

3.3. XPS and Valence Band Spectral Analyses. The survey scans illustrating the various elements prevalent in neat RGO, neat ILFG, PEDOT−RGO, and PEDOT−ILFG are shown in Figure S5, Supporting Information. While neat RGO is primarily composed of C and O, neat ILFG is constituted by C, O, P, F, and N, wherein P and F arise from the ionic liquid anion, tris-(pentafluoroethyl) trifluorophosphate, and N owes its origin to the cation, 1-hexyl-2,3-dimethylimidazolium ion. The general scans of the nanocomposites, in addition to the elements from the neat samples, also include sulfur (S), which stems from the backbone of PEDOT chains (Figure S5c,d, Supporting Information). The formation of neat RGO and neat ILFG was confirmed from their deconvoluted core level spectra shown in Figure S6, Supporting Information. Signals due to C−C, C−OH, C−O−C, C═O, and C(O)O linkages were observed in C1s and O1s spectra for neat RGO. The deconvoluted C1s core level spectrum of neat ILFG showed signals due to C−C, C−N (where N is from the imidazolium ion), C−O, and C−F (the last one from the $\{(C_2F_5)_3PF_3\}^-$ ion). The N1s showed a peak at 397.1 eV, arising from the C−N interaction, wherein C

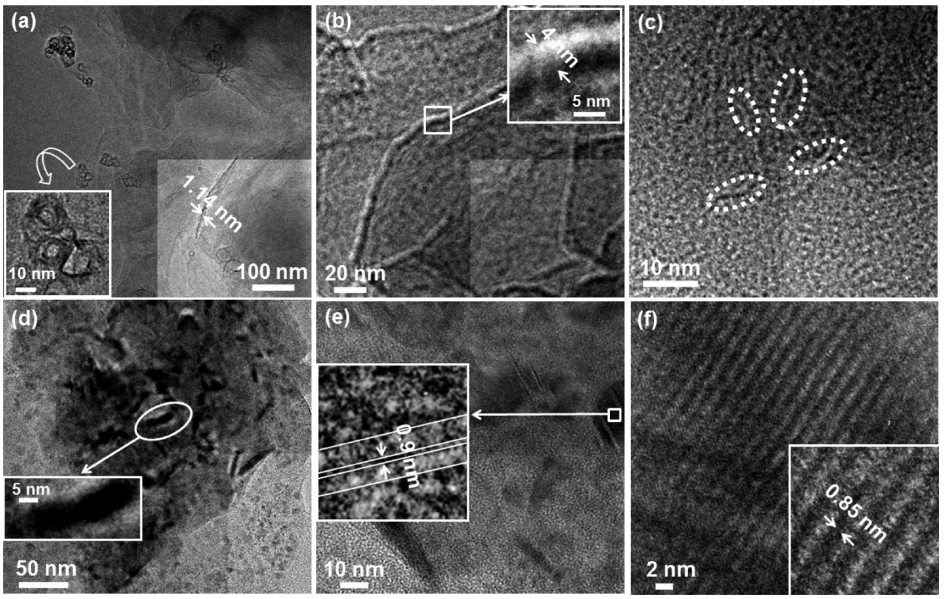

Figure 3. HRTEM micrographs of (a) neat ILFG showing the crumpled sheetlike texture (inset on right-hand side shows the thickness of the nanosheet), (b) neat RGO with the inset showing a blown up view of a fold on the nanosheet, (c) the PEDOT−RGO nanocomposite; the ellipses encircle the streaklike structures typical of RGO and are surrounded by the amorphous polymer, (d) PEDOT−ILFG nanocomposite, the elongated shapes (as in the inset) are characteristic of ILFG, (e) coexisting crystalline and amorphous phases in PEDOT−ILFG (inset is a magnified view of a quasi-ordered arrangement of lattice fringes), and (f) a relatively defect free crystallite of ILFG in PEDOT−ILFG, inset shows the fringe separation of 0.85 nm.

originates from the carbon on graphene nanosheets and N arises from the nitrogens in the imidazolium ring. This peak, in particular, is indicative of the existence of the ionic liquid cations in between the graphene nanosheets. The higher energy peaks at 398.6 and 400.3 eV in the same spectrum are purely from the imidazolium rings, due to the C−N (where N is the neutral nitrogen flanked by three carbons in the imidazolium ion) and due to C−N^+ (where N is tetravalent, again on the imidazolium ring) interactions. For pure alkyl imidazolium based ionic liquids, two similar components were resolved.[40]

In the PEDOT−RGO film, the deconvoluted C1s photoemission (Figure S7a, Supporting Information) yielded peaks due to the C−C from graphene oxide nanosheets/PEDOT, the C−S groups, which is due the sulfur−carbon on the polymer chain, and the C−OH and C═O groups that reside only on the functionalized graphene oxide and not on the polymer. On the other hand, the PEDOT−ILFG nanocomposite film (Figure 4a) comprises seven peaks at 284.6, 285.8, 286.6, 287.5, 288.6, 289.7, and 292.6 eV due to C−C on graphene nanosheets and PEDOT, C−S of PEDOT, C−OH of graphene nanosheets, C−N of ionic liquid functionalized graphene (N from imidazolium ions), C−O−C of graphene nanosheets or PEDOT, C═O of graphene, and C−F from the $\{(C_2F_5)_3PF_3\}^-$ ion. The C−N and C−F components are noteworthy, for N and F stem from the ionic liquid cation and anion, respectively, thus reaffirming that the ionic liquid, as a whole, is an integral part of the PEDOT−ILFG nanocomposite. The O1s signal for both the PEDOT−RGO and PEDOT−ILFG films was composed of three peaks which correspond to the C═O from RGO, C−O of PEDOT, or RGO/ILFG and O−H groups flanked to RGO/ILFG. The core level spectra of S2p for both the films show contributions from the $S2p_{3/2}$ and $S2p_{1/2}$ spin−spin doublet characterized by a fixed 2:1 intensity ratio and with an energy splitting of ∼1.2 eV.[41] In PEDOT−ILFG film (Figure 4c), these arise at 164.5 and 165.7 eV, respectively. The core level spectra of phosphorus (P2p) and fluorine (F1s) are shown in the insets of Figure 4b,d, and these originate from the $\{(C_2F_5)_3PF_3\}^-$ ion of the ionic liquid that is flanked by two adjacent graphene nanosheets in ILFG. The deconvoluted N1s core level spectrum of PEDOT−ILFG film (fwhm = 1.01 eV), shown in Figure 4d, shows three distinct peaks at 397.3, 398.8, and 399.9 eV due to C(of graphene)−N(of imidazolium ion) and due to the ionic liquid moieties, C−N (from the ═N−$CH_2(CH_2)_4CH_3$ group) and C−N^+ (from the ≡N^+−CH_3 group).[40] This is a clear indicator of the fact that the ionic liquid is retained in the film structure even after nanocomposite formation with PEDOT.

The loading of ionic liquid onto the graphene nanosheets, deduced from the {C(of graphene)−N(imidazolium of ionic liquid)} contribution in the deconvoluted N1s spectrum of neat ILFG, is 0.27. This reduces to 0.17 in the PEDOT−ILFG nanocomposite, which is natural, as ILFG is now only an electrochemically inserted counterion flanked to the oxidized polymer chain. The ionic liquid anion, $\{(C_2F_5)_3PF_3\}^-$ loading in the PEDOT−ILFG nanocomposite, is estimated to be ∼0.1, from the $I_{(C-F)}$ component in C1s. For the same material, striking is the value for $I_{(C-O)}$, which is fairly low (∼0.1) as compared to the $I_{(C-C)}$ of 0.55, indicative of a relatively low level of oxidation of the carbon network of graphene nanosheets, whereby the planar two-dimensional structure of sp^2 bonded carbon atoms is largely preserved. In neat RGO, the level of oxidation is rather high as an $I_{(C-O)}$ of ∼0.55 is obtained, which is surprising, as RGO is reduced to graphene oxide. In comparison, the $I_{(C-C)}$ is about 0.44, thus confirming that ionic liquid functionalization is an ideal approach for exfoliating graphite. The doping level of exfoliated reduced graphite in PEDOT−RGO is ∼0.14, obtained from the $I_{(C=O)}/I_{C(total)}$ ratio from the C1s spectrum, and ∼0.15 from the $I_{(C=O)}/I_{C(total)}$ from the O1s spectrum; these are obviously lower than the actual values, as they preclude the C−O

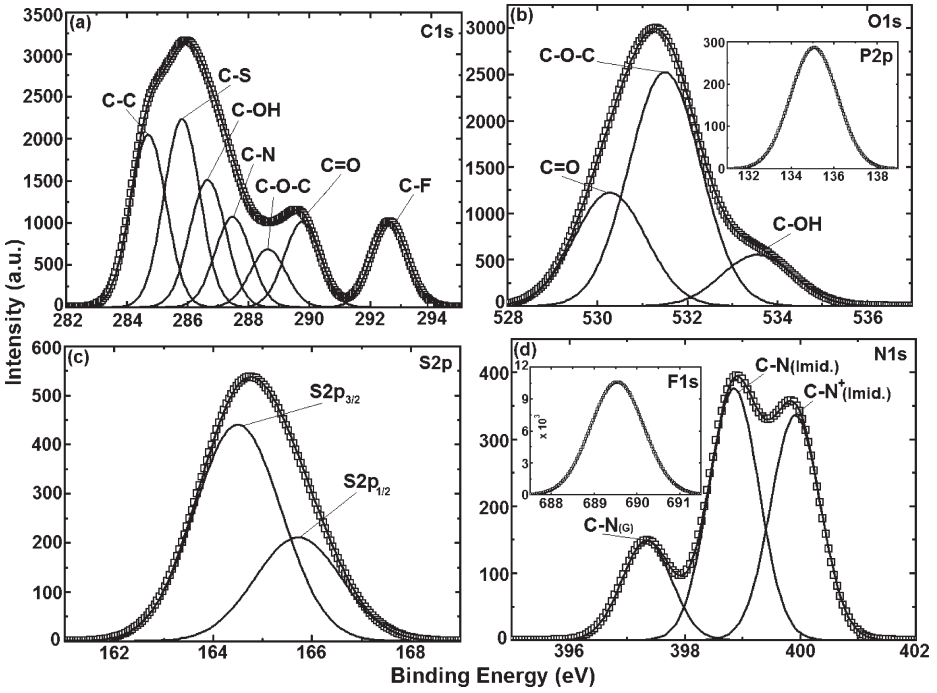

Figure 4. Deconvoluted XPS core level spectra of (a) C1s, (b) O1s, (c) S2p, and (d) N1s of PEDOT−ILFG nanocomposite. Insets of (b) and (d) show the P2p and F1s core level spectra, respectively.

contribution. Since the C−O component, herein, also includes the contribution from PEDOT, it is not reasonable to include the same. Nonetheless, a good agreement is found between the two values obtained from two different spectra (O1s and C1s). EDX (energy dispersive analysis of X-rays) plots of neat ILFG and neat RGO are shown in Figure S8 (Supporting Information) and that of PEDOT−RGO and PEDOT−ILFG are shown in Figure S9, Supporting Information. The EDX analyses also corroborated the greater oxygen content in the ILFG based materials in contrast to RGO based ones.

The density of states near the Fermi level for neat RGO and neat ILFG are displayed in the valence band spectra in Figure 5a. 1D-Graphene is a zero band gap nanomaterial,[42] but here, we deduced a small finite value of 0.43 eV for the Fermi level to valence band gap in neat ILFG, as here graphene is functionalized with ionic liquid or carboxylate groups. This gap was slightly higher for the neat RGO sample (1.48 eV), indicating that ionic liquid functionalization is more conducive for generating a small gap material. For the PEDOT−RGO and the PEDOT−ILFG nanocomposites (Figure 5b and inset), the energy gap between the valence band and the point where the density of states rapidly diminishes are 2.58 and 1.7 eV. The values are close to a reported value of direct optical gap of about 1.8 eV for PEDOT films.[43] Possibly, additional levels are introduced in the composite due to the graphene nanosheets (ILFG), and therefore, band gap decreases, indicating the formation of a more conductive material.

Hydrophobic, nonmiscible ionic liquids like the one used herein, 1-hexyl-2,3-dimethylimidazolium tris(pentafluoroethyl) trifluorophosphate, respond to the addition of water by reorienting their cations to aid in solvating the water molecules.[44] As suggested previously, for a water miscible tetrafluoroborate based ionic liquid,[45] here also, upon application of dc potential (E = +16 V), at the anodic graphite rod, water molecules easily undergo oxidation to yield free radicals, which in turn lead to the formation of oxygen containing functional groups, on the graphene nanosheets.

$$(C)_n + H - O\bullet\bullet H \rightarrow C_{n-1}C - OH + e^- + H^+ \text{(at the anode)} \quad (2)$$

These nanosheets are exfoliated from the anodic rod, upon action of water and potential, which act cumulatively to remove layers of graphene that collapse into the solution. Thus, the graphene generated in the ionic liquid medium also has an oxidized graphene component. Simultaneously, at the cathode, the imidazolium ions undergo reduction and form free radicals, which are easily entrapped by the graphene nanosheets liberated in solution from the anode,[35] as shown in eq 3.

$$(C_{11}H_{21}N_2)^+ + e^- \rightarrow (C_{11}H_{21}N_2)^\bullet \text{(at the cathode)} \quad (3)$$

Noncovalent or $\pi-\pi$ interactions can also form between the imidazolium cation and the graphene nanosheets suspended in the ionic liquid, as shown through eq 4.

$$(C)_n + (C_{11}H_{21}N_2)^+\{(C_2F_5)_3PF_3\}^- \rightarrow (C)_n\text{----}(C_{11}H_{21}N_2)^+\{(C_2F_5)_3PF_3\}^- \text{(in the solution)} \quad (4)$$

All these interactions have been taken into account and are displayed in Figure 6a, the schematic for the PEDOT−ILFG nanocomposite. In case of the PEDOT−RGO nanocomposite, the carboxylate ions on the reduced graphene oxide function as the charge compensating anions and link to the oxidized thiophene rings of PEDOT, as illustrated in Figure 6b.

3.4. I−V Characteristics. The current−voltage ($I-V$) characteristics of neat ILFG have been compared with that of neat RGO in Figure 7a. The variation is almost linear, and the slight

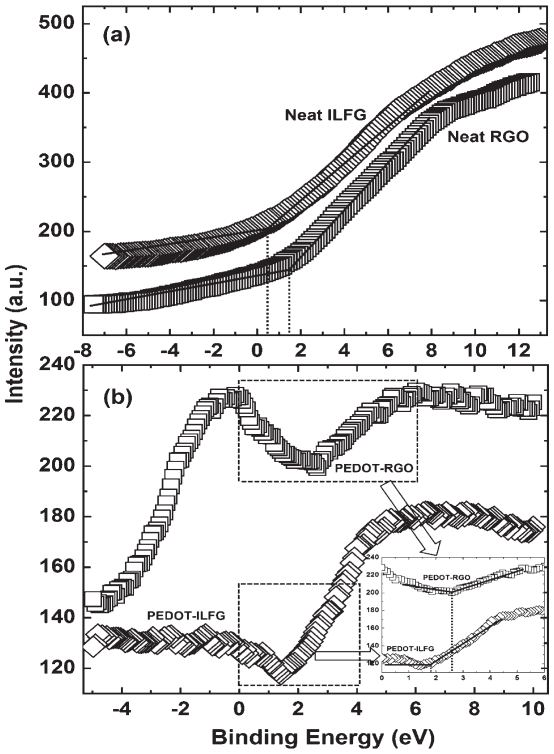

Figure 5. Valence band spectra of (a) neat ILFG (◊) and neat RGO (□) samples and (b) PEDOT−ILFG (◊) and PEDOT−RGO (□) nanocomposite films displaying their respective Fermi edges. Inset of (b) provides a clear view of the valence band to Fermi level gap for the two nanocomposites.

digression from the ohmic response, especially at high bias ($E > +2.1$ V), and the peak observed at +2.65 V in the anodic branch are consistent with a space charge limited current, activated only at high potentials. The injected carriers significantly alter the local electrical field created by the applied potential, under the high biasing condition. A similar peak was observed for the neat RGO sample at a slightly higher potential ($E = +2.72$ V). No saturation of the current was ever observed; instead, the sample resistance decreased gradually at increased dc bias. An $I-V$ response, akin to the one observed herein, was seen earlier for a thermally reduced graphene oxide based field effect device.[46] It is also notable that the neat ILFG is capable of carrying more current as compared to the neat RGO sample for the same values of applied bias, as an I_{max} of 0.53 A is observed for neat ILFG and I_{max} is 0.07 A for the neat RGO at E_{peak} in the anodic branch. In the cathodic sweep, I_{max} coincides with E_{max}, and it is 0.45 A for neat ILFG and 0.05 A for neat RGO at $E = -3$ V. The dc electrical conductivity of neat ILFG, determined from the linear fit, is about 0.6 S cm^{-1}, slightly higher than a value of 0.45 S cm^{-1} obtained for a graphene−silica thin film[47] and again comparable to a conductivity of ∼10 S m^{-1} obtained for a polystyrene−graphene composite[48] but lower than that predicted from $\sigma = 4e^2/h$ and is the attainable lower limiting value for pristine 2D-graphene sheets.[49] The conductivity of the neat RGO sample was only 0.07 S cm^{-1}, which is lower by an order of magnitude than that of neat ILFG. The higher resistance of RGO in comparison to neat ILFG here is due to a greater degree of oxygen-containing groups in the former, which tend to introduce more defects to graphene and lower its conductivity. For the PEDOT−ILFG nanocomposite, again, an E_{peak} was seen at +2.68 V, corresponding to an I_{max} of 0.019 A, whereas for the PEDOT−RGO, the E_{peak} shifted to a more positive potential of +2.92 V and I_{max} was 0.0075 A. I_{max} values showed a similar differential, i.e., by an order of magnitude for the two nanocomposites, in the cathodic branch as well. Conductivity, after forming a composite with PEDOT, reduced to 0.03 S cm^{-1} for PEDOT−ILFG, and it was 9.4 × 10^{-3} S cm^{-1} for the PEDOT−RGO sample. The PEDOT−ILFG conductivity is comparable to a reported σ of ∼0.022 S cm^{-1} for a PEDOT/PSS film[50] and higher than values in the range of 10^{-3}−10^{-7} S cm^{-1} reported for sorbitol treated or pristine PEDOT/PSS samples at temperatures below 100 °C.[51] Our values are even comparable to a σ of 0.07 S cm^{-1} reported for a PEDOT nanowire[52] and again higher by an order of magnitude in comparison to a σ of 2 × 10^{-4} S cm^{-1} reported for PEDOT doped by a sulfonated polyamic acid.[53] It is apparent that graphene nanosheets do play a critical role in increasing the conductivity of PEDOT, for the values are lower when the polymer is doped by conventional salt anions. Further, utilizing functionalized graphene as a counterion is a far more efficient method for improving the conduction pathways in PEDOT, in contrast to the traditional route of ensconcing the polymer in nonaqueous solvents.[53,54]

3.5. Cyclic Voltammetric Studies. The electrochemical behavior of the two nanocomposites was also compared with cyclic voltammetry in the neat ionic liquid: 1-hexyl-2,3-dimethylimidazolium tris(pentafluoroethyl) trifluorophosphate by switching the films between −1.0 and +1.0 V at a sweep rate of 5 mV s^{-1}, as shown in Figure 8a. The PEDOT−ILFG film shows an anodic wave commencing at +0.13 V due to doping by the $\{(C_2F_5)_3PF_3\}^-$ ions, and a cathodic peak in the reverse scan due to dedoping, corresponding to anion extraction, is observed at −0.73 V. A weak shoulder seen at +0.71 V in the voltammogram of PEDOT−ILFG film corresponds to cation extraction from the polymer film, whereas this peak is conspicuously absent in the PEDOT−RGO nanocomposite. It is apparent that anion extraction in the reduction cycle is accompanied by insertion of cations (1-hexyl-2,3-dimethylimidazolium ions) from the electrolyte and charge compensating electrons from the external circuit. This is an indirect evidence for formation of bipolarons in the PEDOT−ILFG film, whereas a similar phenomenon is not inferred from the voltammogram of the PEDOT−RGO nanocomposite. A broad reduction hump was observed in the PEDOT−RGO film ranging from −0.08 to −0.56 V, and the corresponding oxidation hump ranges from −0.02 to +0.28 V; these waves are simply attributable to anion extraction (or neutralization of a polaron by an electron) and insertion (or polaron formation). The curve is similar to that observed previously for a PEDOT film doped by multiwalled carbon nanotubes.[55] Equations illustrating the redox processes in PEDOT−ILFG and PEDOT−RGO nanocomposites are given in Supporting Information.

The maximum cathodic (j_{cmax}) and anodic (j_{amax}) peak current densities observed in the PEDOT−ILFG film are 0.028 and 0.040 mA cm^{-2}, whereas in the PEDOT−RGO nanocomposite, a j_{cmax} of 0.018 mA cm^{-2} and j_{amax} of 0.012 mA cm^{-2} were observed. Furthermore, the amount of charge intercalated and deintercalated in the PEDOT−ILFG film was 9 and 7.1 mC cm^{-2}, respectively, in comparison to 4.5 and 3.6 mC cm^{-2} for the PEDOT−RGO film, thus implying a larger charge storage capacity available to the PEDOT−ILFG film. The dependence of oxidation−reduction phenomena of PEDOT−RGO and PEDOT−ILFG nanocomposites on scan rate are shown in

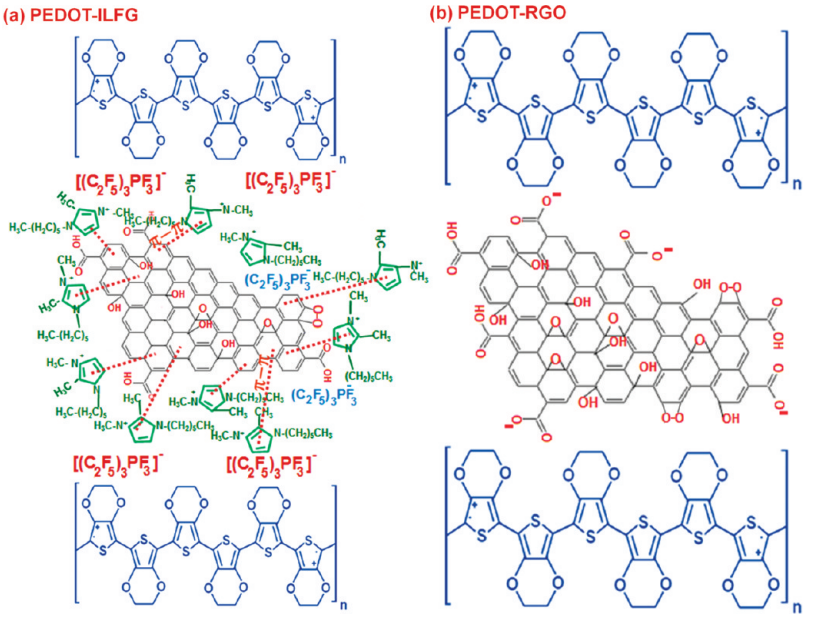

Figure 6. Schematic comparison of the interactions prevalent in (a) PEDOT−ILFG and (b) PEDOT−RGO nanocomposites.

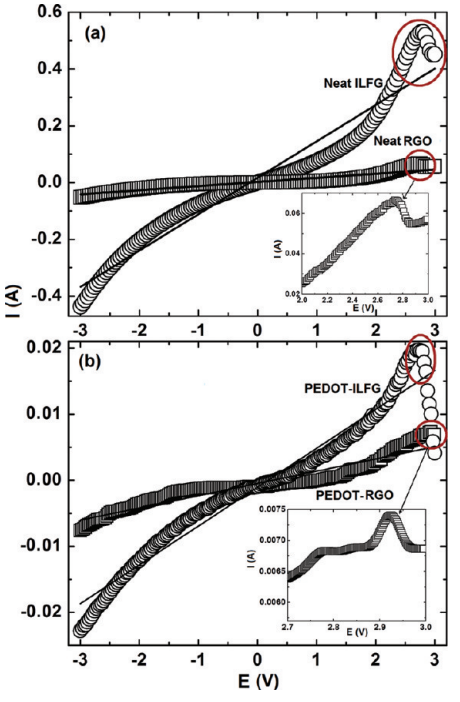

Figure 7. *I*−*V* characteristics of (a) neat ILFG (○) and neat RGO (□) and (b) PEDOT−ILFG (○) and PEDOT−RGO (□) nanocomposites; insets of (a) and (b) are the magnified views to illustrate the digression from the linear trend and peak formation in neat RGO and PEDOT−RGO.

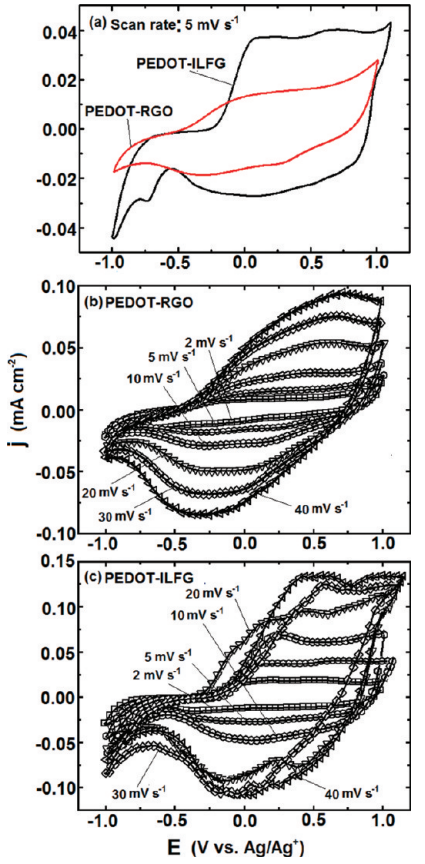

Figure 8. Cyclic voltammograms of (a) PEDOT−RGO and PEDOT−ILFG nanocomposite films recorded at 5 mV s^{-1}. (b) PEDOT−RGO and (c) PEDOT−ILFG nanocomposite films as a function of scan rate: 2, 5, 10, 20, 30, and 40 mV s^{-1}; all in the ionic liquid: 1-hexyl-2,3-dimethylimidazolium tris(pentafluoroethyl) trifluorophosphate.

Figure 8b,c. In the PEDOT−RGO film, a nearly linear relationship between the anodic/cathodic current density maxima with scan rate was perceived, suggesting the presence of surface confined redox active states. The broad oxidation wave shifts to more positive potentials with scan rate (at 5 mV s^{-1}, E (for j_{amax}) = +0.09 V and, at 40 mV s^{-1}, E (for j_{amax}) = +0.68 V). Likewise, in the cathodic branch, the reduction peak also shifts to more negative potentials with increasing scan rate (at 5 mV s^{-1}, E (for j_{cmax}) = −0.26 V and, at 40 mV s^{-1}, E (for j_{cmax}) = −0.31 V).

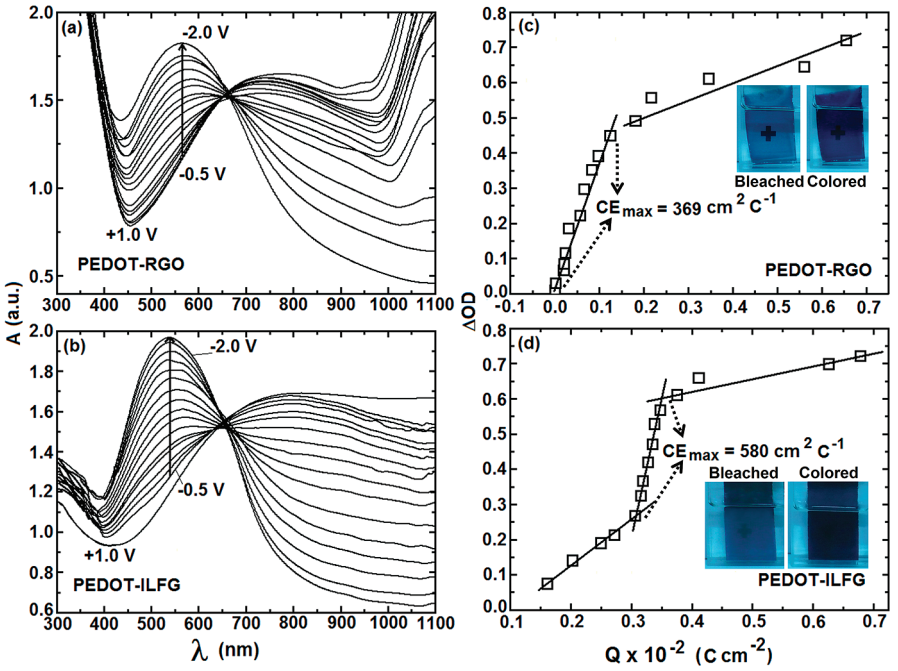

Figure 9. Absorption spectra of (a) PEDOT−RGO and (b) PEDOT−ILFG nanocomposite films recorded under different dc potentials varying from −0.5 to −2.0 V in steps of −0.1 V in the ionic liquid: 1-hexyl-2,3-dimethylimidazolium tris(pentafluoroethyl) trifluorophosphate; the optical state under +1.0 V has been taken as reference for determination of coloration efficiency. Change in optical density versus inserted charge density plots for (c) PEDOT−RGO and (d) PEDOT−ILFG nanocomposite films at a monochromatic wavelength of 550 nm. Insets of (c) and (d) are the same films in dark (−2.0 V) and pale (+1.0 V) blue states.

This shows that anion ingress is hindered at high scan rates, for the time available is not sufficient for efficient anion insertion, and in the reverse cycle, anion egress is inhibited due to the same reason. The behavior of the PEDOT−ILFG nanocomposite was also similar to the one observed in the PEDOT−RGO film, except for the fact that, here, the redox peaks were more prominent, especially at high scan rates of 30 and 40 mV s^{-1}. Notable was the scan recorded at 40 mV s^{-1}, which clearly shows twin reductive components at −0.11 and −0.04 V and a distinct oxidation peak at +0.59 V followed by a plateau in the oxidation sweep. It is ostensible that the graphene oxide nanosheets tend to increase the capacitive characteristics of the PEDOT−RGO film; the broad areas under the cyclic voltammograms of the PEDOT−RGO film are a testimony to this. In the PEDOT−ILFG nanocomposite, the ionic liquid functionalized graphene not only enhances the overall electrochemical activity of the film but also modifies the redox response of the electroactive polymer.

3.6. Spectroelectrochemistry Studies. Typical absorbance plots of PEDOT−RGO and PEDOT−ILFG films recorded as a function of wavelength under different cathodic potentials ranging between −0.5 and −2.0 V are shown in Figure 9. The plots were recorded at intervals of −0.1 V, and E = +1.0 V was utilized as the reference potential for determining the optical density (OD) change for both nanocomposites. In the PEDOT−RGO film (Figure 9a), at a low reduction potential of −0.5 V and in the oxidized state (E = +1.0 V), a broad absorption, corresponding to the bipolaron formation, is visible in the 700−1100 nm wavelength range. The intensity of this peak diminishes progressively as the reduction potential is raised from −0.5 to −1.2 V. At potentials greater than −1.2 V (−2.0 > E (V) > 1.2), a distinct peak corresponding to $\pi-\pi^*$ transitions was observed at ∼550 nm, signaling the neutralization of bipolarons by electrons and formation of the reduced polymer. This peak gains intensity at the expense of the bipolaronic peak, as a function of increasing reduction potential. In the PEDOT−ILFG films (Figure 9b), the bipolaronic peak was observed only up to an E = −0.9 V, and thereafter, the $\pi-\pi^*$ transition peak tends to preponderate. The appearance of this peak at −1.0 V demonstrates that this is the minimum potential to bring about an appreciable change in the optical density in the visible region of the film. In the PEDOT−RGO nanocomposite film, this peak was seen at 562 nm but its intensity was lower than that of the PEDOT−ILFG nanocomposite film for the same value of applied potential, implying that a higher optical density change (ΔOD) can be realized for PEDOT−ILFG films. The absorption edge for the $\pi-\pi^*$ peak of the PEDOT−RGO film (E = −2.0 V) tends to show a blue shift with respect to the same absorption of the PEDOT−ILFG film, at the same potential, which is suggestive of a lower band gap in the PEDOT−ILFG nanocomposite film as compared to the PEDOT−RGO nanocomposite film.

Coloration efficiency (CE or η), which is defined as the optical density change (ΔOD) induced as a function of the injected electronic charge per unit area, i.e., the amount of charge necessary to produce the optical change, is given by

$$\eta(\lambda) = \Delta OD(\lambda)/Q/A \qquad (5)$$

where η (cm^2 C^{-1}) is the coloration efficiency at a given wavelength and ΔOD (λ) = OD (at E = −x V; (x = −0.5 to −2.0)) − OD (E = +1.0 V). Coloration efficiencies of the PEDOT−RGO and PEDOT−ILFG films have been obtained from ΔOD versus injected charge density plots at a monochromatic photopic wavelength of 550 nm (Figure 9c,d). Photographs of the two films displaying their electrochromic contrast

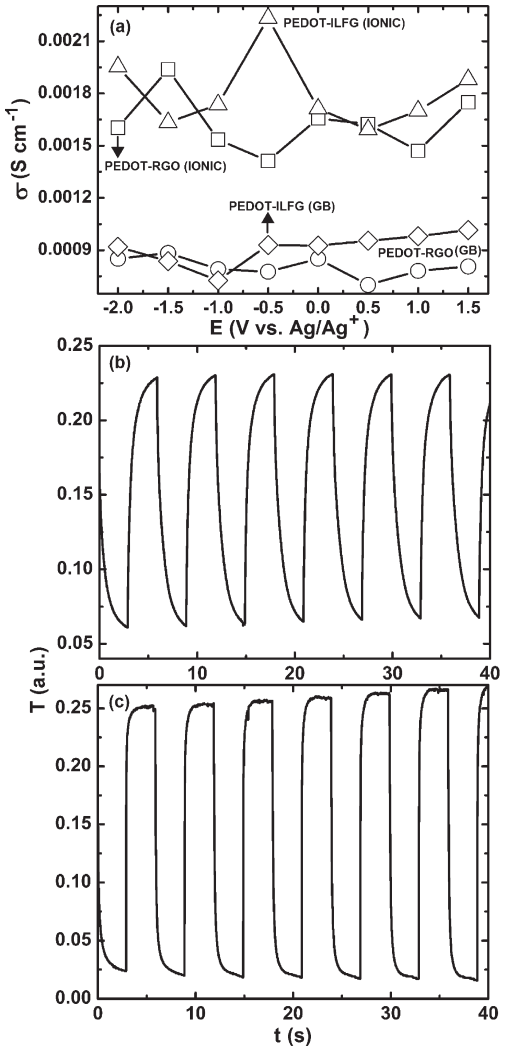

Figure 10. (a) Variation of ionic conductivity and grain-boundary conductivity as a function of applied dc potential of PEDOT−RGO (□,○) and PEDOT−ILFG (△,◇) nanocomposite films. Variation of transmittance at a monochromatic wavelength of 632.8 nm as a function of time for (b) PEDOT−RGO and (c) PEDOT−ILFG films under a square wave dc potential of ±1.5 V at a frequency of 0.16 Hz.

are shown in the insets of Figure 9c,d. In accordance with the absorption plots, the PEDOT−ILFG film has a deeper color in the colored state than the PEDOT−RGO film, for the same bias. The PEDOT−RGO nanocomposite shows two slopes: the first one corresponding to an intercalated charge density of 0−1.2 mC cm^{-2} yields a CE of 369 cm^2 C^{-1}, and the second slope in the range of 1.7−6.4 mC cm^{-2} manifests in a CE of 53 cm^2 C^{-1}. In the PEDOT−ILFG nanocomposite, the plot can be split into three slopes corresponding to charge density ranges of 1.6−3.1, 3−3.5, and 3.5−6.8 mC cm^{-2}, yielding CE of 33, 580, and 129 cm^2 C^{-1}, respectively. The PEDOT−RGO film shows a higher CE at low charge intercalation levels, while the reverse is true for the PEDOT−ILFG film. This value is higher than a CE of 206 cm^2 C^{-1} reported for PEDOT or a value of 428 cm^2C^{-1} achieved for a PProDOT-Me_2 (poly(propylenedioxythiophene)) film at a λ_{max} of 585 nm.[56] However, our value is lower than a CE of 680 cm^2 C^{-1} (λ = 535 nm) reported for (Bis-PEDOT)-methoxy ethyl hexyl benzene or an exceedingly high value of 1365 cm^2 C^{-1} obtained for PProDOT-$(Bu)_2$ at λ = 576 nm.[57,58] It is apparent that the PEDOT−ILFG film is able to utilize the intercalated charge more efficiently than the PEDOT−RGO film, by the virtue of a greater number of electrochemically addressable sites, which translates into a higher coloration efficiency in the former.

3.7. EIS Investigations. The variation of both ionic and grain boundary conductivities determined from the diameters of impedance arcs are shown as a function of applied potential in Figure 10a. The corresponding Nyqvist plots are shown in Figure S10, Supporting Information. A similar approach has been applied to polypyrrole films before by Pickup et al.,[59−62] and it was established as a fairly reliable method for deducing ionic conductivities of conducting polymers. Some points that warrant attention are (i) at a given bias, the ionic conductivity is greater than the grain boundary conductivity by almost an order of magnitude, be it the PEDOT−RGO or PEDOT−ILFG nanocomposite, (ii) the largest differential between the ionic conductivities of PEDOT−RGO (σ_i = 0.0014 S cm^{-1}) and PEDOT−ILFG (σ_i = 0.0022 S cm^{-1}) is observed under −0.5 V, and (iii) third, σ_{gb} is higher under oxidation potentials, as compared to its values under reduction potentials for the PEDOT−ILFG nanocomposite (albeit the value at −0.5 V). The dc conditioning of E = −0.5 V results in anomalous behavior, as ionic conductivities are comparable at other reduction and oxidation potentials, for both PEDOT−ILFG and PEDOT−RGO nanocomposites. During oxidation, electrons are transported across the film to the SnO_2−F/PEDOT interface through a polaron hopping mechanism while anions are transported across the film from the PEDOT/electrolyte interface. An electron jumps from a reduced site to an adjacent oxidized site, and the counterion moves in the opposite direction, for charge compensation. Owing to these two opposing effects, under oxidation potentials of +0.5 and +1 V, the ionic conductivities are lower for both PEDOT−ILFG and PEDOT−RGO, in comparison to the corresponding σ_i at 0 V. Only at E = +1.5 V, σ_i for the two nanocomposites is higher than their respective values at E = 0 V, which is a natural consequence of potential activated conduction. During reduction, electrons occupy the oxidized sites across the film, and anions are transported to the electrolyte; it appears as if the two fluxes act in the same direction. Consequently, ionic conduction is unimpeded, and at the first reduction potential of −0.5 V, the ionic conductivity is higher than that at E = 0 V for the PEDOT−ILFG nanocomposite. However, for the PEDOT−RGO nanocomposite, this effect was observed only at a much higher reduction potential of −1.5 V, which is an indirect indicator of facile ion-transport in the PEDOT−ILFG nanocomposite. For poly(methylpyrrole), ionic conductivity was of the order of 312 μS cm^{-1}.[60] Our values for σ_i agree reasonably well with the reported values for analogous systems. The grain boundary conductivity is about 900 μS cm^{-1} for PEDOT−ILFG in the potential range of −0.5 to +2 V. This σ_{gb} reduces to 726 and 836 μS cm^{-1} under −1 and −1.5 V, respectively, and again rises to 919 μS cm^{-1} at −2 V, indicating that, during oxidation and at low reduction levels, grain boundaries act to facilitate anion insertion whereas they obstruct anion extraction during reduction. For the PEDOT−RGO nanocomposite, the σ_{gb} values increase with potential, from 776 to 880 μS cm^{-1} ongoing from −0.5 to −1.5 V and from 700 to 806 μS cm^{-1} ongoing from +0.5 to +1.5 V. It is apparent that the external bias acts as a driving force for fast conduction in this sample.

3.8. Switching Kinetics. The color-bleach characteristics of the films recorded at 632.8 nm under a square wave potential of ±1.5 V at an optimized frequency of 0.16 Hz (equivalent to a step time of 3 s for each half cycle) are shown in Figure 10b. The switching kinetics was examined by evaluating the time taken for a 100% transmission change corresponding to an absolute optical contrast for the films of same thickness and geometric area. First, for the PEDOT−RGO film, the total contrast is only 71.5% of that achieved for the PEDOT−ILFG film. The time taken for transmission to increase from 0 to 100% or bleaching is 1.3 s and for coloration or a transmittance change of 100 to 0% occurs in 3 s. For a 90% transmittance change (for % *T* to decrease from 90 to 10%), the time required is 1.3 s and the corresponding bleaching time (for % *T* raise from 10 to 90%) is 0.5 s. For the PEDOT−RGO film, both coloration and bleaching times are equal; both processes occur in 3 s each, but contrary to the PEDOT−ILFG film, where bleaching saturates immediately, upon the change of polarity, and coloration saturation is time-consuming, in the PEDOT−RGO film, at the same frequency, neither the bleached nor the colored states saturate. It is evident that a larger number of electrochemically active sites prevail in the PEDOT−ILFG nanocomposite film which manifests in a larger amplitude of optical contrast. Further, the internal resistance of the film is also lower than that of the PEDOT−RGO film, which is reflected in the faster switching kinetics or faster ion movement shown by the former. Our values are comparable to coloration times of 1.3−3.1 s and superior to bleaching times of 1.2−2.7 s (corresponding to a 90% switch) reported for poly(hexyl viologen)−PEDOT/PSS based layer-by-layer grown assemblies[63] and also comparable to switching times in the range of 1.2−0.8 s reported for a PEDOT−poly(methyl thiophene) device.[64] However, our values are lower than that reported for a PEDOT nanotube based device, for which reversible transitions between dark to colorless occurred in a few milliseconds.[65] A larger geometric area and a bulkier anion used herein could be plausible reasons for slower kinetics.

CONCLUSIONS

Graphene nanosheets separated by 1-hexyl-2,3-dimethylimidazolium tris(pentafluoroethyl) trifluorophosphate, generated by exfoliation of graphite rods in the same, and graphene oxide prepared by the traditional Hummers' route when used as electrolytes, for electropolymerization of EDOT, served as counterions and were impregnated in the ensuing polymer deposit to yield PEDOT−ILFG and PEDOT−RGO nanocomposite films. Broadened carbon signals and a distinctive carbon−nitrogen signal corresponding to the imidazolium−graphene nanosheet interaction confirmed the successful incorporation of the ionic liquid in the PEDOT−ILFG nanocomposite. HRTEM also revealed the presence of lattice fringes corresponding to graphene in the PEDOT−ILFG nanocomposite with an interplanar spacing of 0.85 nm. Folded/graphene nanosheets amalgamated with the disordered/wrinkled polymer were achieved in PEDOT−RGO. The significantly lowered level of oxidation in ILFG in comparison to the oxidation level in RGO affirmed the dual power of a hydrophobic ionic liquid as a medium/functionalizing agent for exfoliating graphite to yield graphene nanosheets with a profoundly intact carbon structure, in a noninert atmosphere at ambient temperature. Amplified redox activity, faster switching kinetics, larger optical modulation, a much superior electronic conductivity, a relatively lower valence band to Fermi level gap, and a considerably improved electrochromic coloring efficiency in PEDOT−ILFG as compared to PEDOT−RGO reiterate the role of graphene nanosheets in facilitating electron/charge transport through the films.

ASSOCIATED CONTENT

Supporting Information. Cross-sectional SEM views and AFM images of PEDOT−RGO and PEDOT−ILFG films, pictures for exfoliation of graphite rods, TEM and SEM images of neat ILFG, XPS survey scans of neat ILFG, neat RGO, PEDOT−RGO, and PEDOT−ILFG films, deconvoluted core level spectra of neat RGO, neat ILFG, and PEDOT−RGO nanocomposite film, EDX patterns of neat RGO, neat ILFG, PEDOT−RGO, and PEDOT−ILFG, and Nyqvist plots of PEDOT−RGO and PEDOT−ILFG films recorded under different potentials. This information is available free of charge via the Internet at http://pubs.acs.org/.

AUTHOR INFORMATION

Corresponding Author

*Fax: +91-40-23016003. Tel: +91-40-23016024. E-mail: mdeepa@iith.ac.in.

ACKNOWLEDGMENT

Financial support from Department of Science and Technology (DST/TSG/PT/2007/69) is gratefully acknowledged.

REFERENCES

(1) Prasad, K. R.; Munichandraiah, N. *Electrochem. Solid State Lett.* **2002**, *5*, A271–A274.
(2) Stenger-Smith, J. D.; Webber, C. K.; Anderson, N.; Chafin, A. P.; Zong, K.; Reynolds, J. R. *J. Electrochem. Soc.* **2002**, *149*, A973–A977.
(3) Romero, P. G.; Chojak, M.; Cuentas-Gallegos, K.; Asensio, J. A.; Kulesza, P. J.; Casan-Pastor, N.; Lira-Cantu, M. *Electrochem. Commun.* **2003**, *5*, 149–153.
(4) Brahim, S.; Wilson, A. M.; Narinesingh, D.; Iwuoha, E.; Guiseppi-Elie, A. *Microchim. Acta* **2003**, *143*, 123–137.
(5) Forzani, E. S.; Zhang, H.; Nagahara, L. A.; Amlani, I.; Tsui, R.; Tao, N. *Nano Lett.* **2004**, *4*, 1785–1788.
(6) Thomas, S. W.; Joly, G. D.; Swager, T. M. *Chem. Rev.* **2007**, *107*, 1339–1386.
(7) Hatchett, D. W.; Josowicz, M. *Chem. Rev.* **2008**, *108*, 746–769.
(8) Novak, P.; Muller, K.; Santhanam, K. S. V.; Haas, O. *Chem. Rev.* **1997**, *97*, 207–281.
(9) Nogueira, A. F.; Longo, C.; Paoli, M. A. D. *Coord. Chem. Rev.* **2004**, *248*, 1455–1468.
(10) Hou, Y.; Cheng, Y.; Hobson, T.; Liu, J. *Nano Lett.* **2010**, *10*, 2727–2733.
(11) Heo, J.; Oh, J.-W.; Ahn, H.-I.; Lee, S.-B.; Cho, S.-E.; Kim, M.-R.; Lee, J.-K.; Kim, N. *Synth. Met.* **2010**, *160*, 2143–2150.
(12) Tallman, D. E.; Spinks, G.; Dominis, A.; Wallace, G. G. *J. Solid State Electrochem.* **2002**, *6*, 73–84.
(13) Pernaut, J. M.; Reynolds, J. R. *J. Phys. Chem. B* **2000**, *104* 4080–4090.
(14) Bayon, R.; Musembi, R.; Belaidi, A.; Bar, M.; Guminskaya, T.; Lux-Steiner, M. C.; Dittrich, T. *Sol. Energy Mater. Sol. Cells* **2005**, *89*, 13–25.
(15) Lock, J. P.; Lutkenhaus, J. L.; Zacharia, N. S.; Im, S. G.; Hammond, P. T.; Gleason, K. K. *Synth. Met.* **2007**, *157*, 894–898.
(16) Ikushima, K.; John, S.; Ono, A.; Nagamitsu, S. *Synth. Met.* **2010**, *160*, 1877–1883.
(17) Okuzaki, H.; Suzuki, H.; Ito, T. *Synth. Met.* **2009**, *159*, 2233–2236.

(18) Argun, A. A.; Cirpan, A.; Reynolds, J. R. *Adv. Mater.* **2003**, *15*, 1338–1341.
(19) DeLongchamp, D.; Hammond, P. T. *Adv. Mater.* **2001**, *13* 1455–1459.
(20) Groenendaal, L. B.; Jonas, F.; Freitag, D.; Pielartzik, H.; Reynolds, J. R. *Adv. Mater.* **2000**, *12*, 481–494.
(21) Deepa, M.; Awadhia, A.; Bhandari, S. *Phys. Chem. Chem. Phys.* **2009**, *11*, 5674–5685.
(22) Zhou, Y. K.; He, B. L.; Zhou, W. J.; Huang, J.; Li, X. H.; Wu, B.; Li, H. L. *Electrochim. Acta* **2004**, *49*, 257–262.
(23) Zengin, H.; Zhou, W.; Jin, J.; Czerw, R.; Smith, D. W.; Echegoyen, L.; Carroll, D. L.; Foulger, S. H.; Ballato, J. *Adv. Mater.* **2002**, *14*, 1480–1483.
(24) Saito, Y.; Uemura, S.; Hamaguchi, K. *Jpn. J. Appl. Phys.* **1998**, *37*, L346–L348.
(25) Bhandari, S.; Deepa, M.; Srivastava, A. K.; Lal, C.; Kant, R. *Macromol. Rapid Commun.* **2008**, *29*, 1959–1964.
(26) Bhandari, S.; Deepa, M.; Srivastava, A. K.; Joshi, A. G.; Kant, R. *J. Phys. Chem. B* **2009**, *113*, 9416–9428.
(27) Bhandari, S.; Deepa, M.; Sharma, S. N.; Joshi, A. G.; Srivastava, A. K.; Kant, R. *J. Phys. Chem. C* **2010**, *114*, 14606–14613.
(28) Park, S.; Ruoff, R. S. *Nat. Nanotechnol.* **2009**, *58*, 217–224.
(29) Wang, D. W.; Li, F.; Zhao, J.; Ren, W.; Chen, Z. G.; Tan, J.; Wu, Z. S.; Gentle, I.; Lu, G. Q.; Cheng, H. M. *ACS Nano* **2009**, 3, 1745–1752.
(30) Wang, Y.; Kurunthu, D.; Scott, G. W.; Bardeen, C. J. *J. Phys. Chem. C* **2010**, *114*, 4153–4159.
(31) Xu, Y.; Wang, Y.; Liang, J.; Huang, Y.; Ma, Y.; Wan, X.; Chen, Y. *Nano Res.* **2009**, *2*, 343–348.
(32) Chang, H.; Wang, G.; Yang., A.; Tao, X.; Liu, X.; Shen, Y.; Zheng, Z. *Adv. Funct. Mater.* **2010**, *20*, 2893–2902.
(33) Choi, K. S.; Liu, F.; Choi, J. S.; Seo, T. S. *Langmuir* **2010**, *26* (15), 12902–12908.
(34) Su, Q.; Pang, S.; Alijani, V.; Li, C.; Feng, X.; Mullen, K. *Adv. Mater.* **2009**, *21*, 3191–3195.
(35) Liu, N.; Luo, F.; Wu, H.; Liu, Y.; Zhang, C.; Chen, J. *Adv. Func. Mater.* **2008**, *18*, 1518–1525.
(36) Hummers, W. S., Jr.; Offeman, R. E. *J. Am. Chem. Soc.* **1958**, *80*, 1339–1339.
(37) Randriamahazaka, H. *J. Electroanal. Chem.* **1999**, *472*, 103–111.
(38) Gao, W.; Alemany, L. B.; Ci, L.; Ajayan, P. M. *Nat. Chem.* **2009**, *1*, 403–408.
(39) Sonmez, G.; Schottland, P.; Reynolds, J. R. *Synth. Met.* **2005**, *155*, 130–137.
(40) Ikari, T.; Keppler, A.; Reinmoller, M.; Beenken, W. J. D.; Krischok, S.; Marschewski, M.; Maus-Friedrichs, W.; Hofft, O.; Endres, F. *e-J. Surf. Sci. Nanotech.* **2010**, *8*, 241–245.
(41) Li, C.; Imae, T. *Macromolecules* **2004**, *37*, 2411–2416.
(42) Avouris, P.; Chen, Z.; Perebeinos, V. *Nat. Nanotechnol.* **2007**, *2*, 605–615.
(43) Kumar, A.; Reynolds, J. R. *Macromolecules* **1996**, *29*, 7629–7630.
(44) Rivera-Rubero, S.; Baldelli, S. *J. Am. Chem. Soc.* **2004**, *126* 11788–11789.
(45) Lu, J.; Yang, J. X.; Wang, J.; Lim, A.; Wang, S.; Loh, K. P. *ACS Nano* **2009**, *3*, 2367–2375.
(46) Jung, I.; Dikin, D. A.; Piner, R. D.; Ruoff, R. S. *Nano Lett.* **2008**, *8*, 4283–4287.
(47) Watcharotone, S.; Dikin, D. A.; Stankovich, S.; Piner, R.; Jung, I.; Dommett, G. H. B.; Evmenenko, G.; Wu, S. E.; Chen, S. F.; Liu, C. P.; Nguyen, S. T.; Ruoff, R. S. *Nano Lett.* **2007**, *7*, 1888–1892.
(48) Stankovich, S.; Dikin, D. A.; Dommett, G. H. B.; Kohlhaas, K. M.; Zimney, E. J.; Stach, E. A.; Piner, R. D.; Nguyen, S. T.; Ruoff, R. S. *Nature* **2006**, *442*, 282–286.
(49) Hwang, E. H.; Adam, S.; Sarma, S. D. *Phys. Rev. Lett.* **2007**, *98*, 186806–186809.
(50) Dimitriev, O. P.; Grinko, D. A.; Noskov, Y. V.; Ogurtsov, N. A.; Pud, A. A. *Synth. Met.* **2009**, *159*, 2237–2239.
(51) Nardes, A. M.; Kemerink, M.; Kok, M. M. D.; Vinken, E.; Maturova, K.; Janssen, R. A. J. *Org. Elec.* **2008**, *9*, 727–734.
(52) Samitsu, S.; Iida, T.; Fujimori, M.; Heike, S.; Shimomura, T.; Ito, K. *Synth. Met.* **2005**, *152*, 497–500.
(53) Somboonsub, B.; Invernale, M. A.; Thongyai, S.; Praserthdam, P.; Scola, D. A.; Sotzing, G. A. *Polymer* **2010**, *51*, 1231–1236.
(54) Timpanaro, S.; Kemerink, M.; Touwslager, F. J.; Kok, M. M. D.; Schrader, S. *Chem. Phys. Lett.* **2004**, *394*, 339–343.
(55) Peng, C.; Jin, J.; Chen, G. Z. *Electrochim. Acta* **2007**, 53, 525–537.
(56) Gaupp, C. L.; Welsh, D. M.; Rauh, R. D.; Reynolds, J. R. *Chem. Mater.* **2002**, *14*, 3964–3970.
(57) Sonmez, G.; Meng, H.; Wudl, F. *Chem. Mater.* **2004**, *16*, 574–580.
(58) Reeves, B. D.; Grenier, C. R. G.; Argun, A. A.; Cirpan, A.; McCarley, T. D.; Reynolds, J. R. *Macromolecules* **2004**, *37*, 7559–7569.
(59) Ren, X.; Pickup, P. G. *J. Phys. Chem.* **1993**, *97*, 5356–5362.
(60) Ren, X.; Pickup, P. G. *J. Chem. Soc. Faraday Trans.* **1993**, *89* 321–326.
(61) Pickup, P. G. *J. Chem. Soc. Faraday Trans.* **1990**, *86*, 3631–3636.
(62) Macdonald, J. R. In *Impedance Spectroscopy Emphasizing Solid Materials and Systems*; Wiley-Interscience: New York, 1987.
(63) DeLongchamp, D. M; Kastantin, M.; Hammond, P. T. *Chem. Mater.* **2003**, *15*, 1575–1586.
(64) Ma, L.; Li, Y.; Yu, X.; Yang, Q.; Noh, C. *Sol. Energy Mater. Sol. Cells* **2009**, *93*, 564–570.
(65) Cho, S. I.; Choi, D. H.; Kim, S. H.; Lee, S. B. *Chem. Mater.* **2005**, *17*, 4564–4566.